Variational Methods and Periodic Solutions
Proceedings of the Symposium on Celestial Mechanics and N-body Dynamics, 2011
Eds. M. Saito, M. Shibayama and M. Sekiguchi

近地球小惑星の定常流による非対称なクレーター形成
Asymmetric lunar cratering by a steady-state NEA flux model

伊藤孝士 [1]
Takashi Ito
自然科学研究機構国立天文台天文シミュレーションプロジェクト
CfCA, National Astronomical Observatory of Japan, NINS

Abstract. 昨今の月探査の成果より、月面に於ける若い光条クレーターが月の前面と後面で非対称的に分布することが分かっている。この非対称性は月の同期回転に起因している。本研究では近地球天体とりわけ近地球小惑星と惑星・月との衝突確率に関する制限多体数値実験により、この月面クレーター非対称分布に関する詳細な調査を行った。近地球小惑星が月や地球型惑星と衝突する場合の衝突確率、衝突速度・衝突角度の分布を計算し、最終的にはクレーター記録との照合が目標である。私達は従来の研究よりも詳細な計算を行い、近地球小惑星と地球型惑星との衝突確率とその時間変化を測定した。私達自身の研究も含めた先行研究と本研究との最も大きな違いは、今回の計算では近地球小惑星の定常フラックスモデルを用いたことである。現実の太陽系に於いては近地球小惑星は常にメインベルトから供給されているので、それを模擬した定常フラックスを導入することは力学モデル全体を現実化することの一助となる。また、近地球小惑星としては実際に検出されている Apollo, Amor, Aten 群の天体でも数値実験を行った。計算結果としては近地球小惑星が月面に作る前面と後面のクレーター数密度比はまだ小さく、月面の光条クレーターの観測が示している数値 ($\sim$1.67) とはまだ乖離があることが判明した。

The asymmetric cratering on satellites is generally related to the synchronous rotation of satellites. On the Moon, the asymmetric distribution of craters has been ascribed to the impacts of the near-Earth asteroid (NEA) population. However, the observed rayed crater distribution's asymmetry on the Moon stared from a debiased NEA population is significantly more pronounced than what

[1]ito.t@nao.ac.jp

had been predicted by previous numerical studies. This suggests the existence of an undetected population of slower (low impact velocity) projectiles. In this paper, as an extension of our previous trials, we carried out numerical simulations of the orbital evolution of NEA-like particles generated from a new NEA flux model which contains substantial amount of high-inclination component as well as close-Earth component. We tried to determine their impact flux on the Moon and resulting asymmetric distribution of craters. The new model is considered to be closer to "true" distribution of NEAs than the conventional NEA flux model is. As a result we obtained slightly enhanced degree of cratering asymmetry from the new model. But it is not quite different from what the conventional model had yielded: The discrepancy between the observational crater record remains. Existence of more, slower objects is still implied from the current result.

1. Introduction

Many planetary satellites are locked in synchronous rotation, and their mean rotational angular speed and mean orbital motion is in a 1:1 commensurability. The synchronous rotation of these satellites leads to asymmetric spatial distribution of impact craters on these satellites: the leading hemisphere tends to have more craters than the trailing hemisphere, as is observed on the Galilean satellites of Jupiter, on Neptune's moon Triton, and on the Moon around the Earth (Shoemaker et al. 1982; Horedt & Neukum 1984; Schenk & Sobieszczyk 1999; Zhanle et al. 1998; Zahnle et al. 2011). Particularly, the asymmetric cratering on the Moon (Morota & Furumoto 2003; Werner & Medvedev 2010) is quite interesting because it reflects the steady-state of modern near-Earth asteroids (NEAs) impact flux recorded on morphologically young and fresh craters with bright rays, called rayed craters (McEwen et al. 1997). In Morota & Furumoto (2003), the observed ratio of crater density ($D > 5$ km) at the apex to that at the antapex is shown to be ~ 1.65. In addition, there is a recent report that small seismic events observed by the Apollo mission can be used to obtain information of the current lunar bombardments with small magnitude (Kawamura et al. 2011). In Kawamura et al. (2011), the number density ratio of the seismic events of roughly 1.4–1.9 has been reported between leading and trailing sides.

The degree of the leading/trailing asymmetric crater distribution on a synchronized satellite orbiting its mother planet is a function of satellite's orbital velocity and the average relative velocity between projectiles and the satellite–planet system. When a satellite with a synchronous rotation has a large orbital velocity around its mother planet, or when the average relative velocity between projectiles and the planet–satellite system is small, the asymmetric distribution of craters becomes the most remarkable. Smaller orbital velocity of the satellite, or larger average relative velocity of projectiles, tends to diminish the asymmetry of crater distribution.

For the purpose to quantitatively test the hypothesis that impacts from the NEA population account for the observed asymmetric crater distribution on the Moon, in the past we had simulated numerically the spatial distribution of impacts of NEAs, using a numerical model with a steady-state population of impactors based on current estimates of debiased near-Earth asteroid population (Ito & Malhotra 2010). Starting from the population of NEAs that had been through a debiased processing process (Bottke et al. 2000, 2002), we had compared the results of the simulation with the observed asymmetry of the population of rayed craters on the leading/trailing hemispheres of the Moon. Our numerical simulation had yielded a leading/trailing hemispherical ratio of $\sim$1.32 for lunar impacts by NEAs, which is only marginally compatible with the observed ratio of $\sim$1.65 found by the geological observation (Morota & Furumoto 2003). For a comparison test, we carried out another set of numerical integrations of the raw, not debiased population of NEAs, expecting to contain more slower objects that can produce higher asymmetric cratering than the debiased population (Ito 2011). However the resulting asymmetry turned out to be $\sim$1.37, not as high as the observed asymmetry deduced from the rayed crater record. A possible explanation for the discrepancies is that there exists a hitherto undetected population of small objects whose average impact velocities on the Moon are much lower than the average impact velocity of the known NEA population. Other explanations are possible, including the possibility that a more comprehensive study of young lunar craters could reveal a smaller leading/trailing asymmetry and thereby remove the discrepancy with the dynamical modeling.

In this paper, as an extension of our previous studies (Ito & Malhotra 2010; Ito 2011), we carried out yet another set of numerical integrations of an NEA population including a different type of component: particles with higher inclination and smaller semimajor axis. The population is created through a synthetic NEA model that is based on the most credible basis of NEA dynamics and observation to date. Our numerical experiment in this

paper will serve as a check as to how differently debiasing models work on changing the impact velocity distribution and asymmetric impacts of the Earth/Moon colliding projectiles.

In Section 2. we describe our model, method, and our choice of initial conditions. Our results on NEA encounters and collisions with the Earth–Moon system are given in Section 3.. This section includes the result about the NEA impact fluxes, impact velocities and their spatial distribution on the Moon. In Section 4. we compare our numerical result with the actual observation record. Section 5. goes for some discussion.

2. Initial conditions and numerical model

Our numerical model follows that in Ito (2011), having two stages. In the first stage, our numerical integrations include the eight major planets and the Sun, and a large number of test particles with NEA-like orbits (Fig. 1). We numerically integrate their orbital evolution for up to 100 million years. Throughout these integrations, we record all close encounters of the particles that reach the Earth's activity sphere (see Section 3. for more detail). We use this record in our second stage of numerical simulation, in which we adopt the restricted N-body model consisting of the Earth, the Moon, the Sun, and cloned test particles within the Earth's activity sphere. In the second stage, we do not include the effects of any planets except the Earth but we include the Moon's gravity. Our aim and numerical method are similar to those in what was published in previous literatures as numerical (Gallant et al. 2009) or analytical (Le Feuvre & Wieczorek 2008, 2011) work, but we believe our model is more realistic and straightforward.

For our first stage numerical simulation in this paper we used two different populations of NEA-like particles. Both from the synthetic, "debiased" NEA population models, but one of them is a conventional model, and the other is a revised one.

The conventional NEA model (hereafter called the population A) was devised in Bottke et al. (2002). This is also the model that we consulted as standard in our previous studies (Ito & Malhotra 2010; Ito 2011). The NEA population described by this model is assumed to be continuously supplied from five intermediate source regions: the ν_6 secular resonance in the main asteroid belt, the 3:1 mean motion resonance at 2.5 AU, the intermediate source Mars-crossers, the outer main belt, and the trans-Neptunian disk. This model is established by taking a linear combination of the (a, e, I) distributions from each of the source regions with best fit parameters based on the Spacewatch observation. The set of the population A particles in this

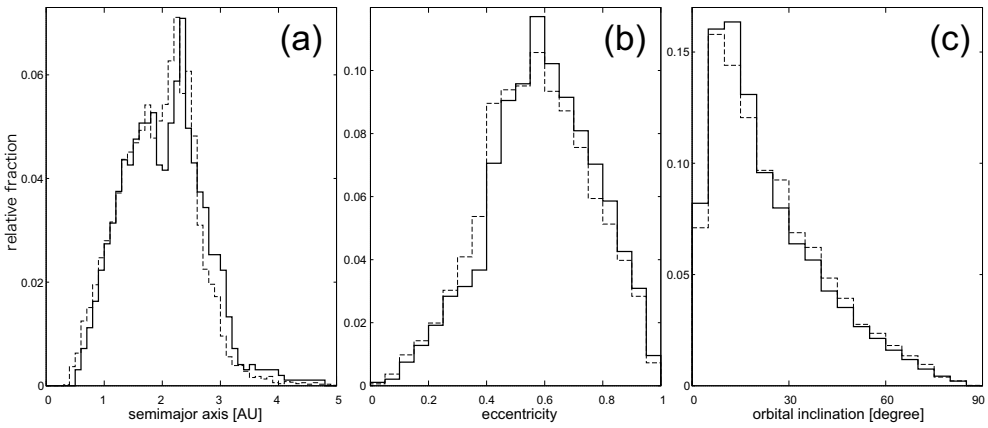

Figure 1. Initial distribution of the osculating orbital elements of the NEA population in our numerical model of the first stage. (a) Semimajor axis, (b) eccentricity, and (c) orbital inclination. The solid lines are for the population A particles, and the dashed lines are for the population B particles.

paper has an orbital distribution that obeys the histograms shown in Figure 12 of Bottke et al. (2002) which gives the debiased orbital distribution of the near-Earth asteroids of absolute magnitude $H < 18$. We produced 18,000 particles along with this distribution and used for the numerical integrations described in the next sections.

On the other hand, there is another numerical NEA model which we hereafter call the population B. This model is not yet officially published, but mentioned and described in detail in Moon et al. (2008), referred to as a model by "Morbidelli (2006, personal communication)". Basically this new model is an updated version of the conventional model with the help of observational bias correction of NEAs (Stuart 2004; Stuart & Binzel 2004), adding two more high inclination sources such as Hungaria ($1.77 < a < 2.06$AU, $I > 15°$) and Phocaeas ($2.1 < a < 2.5$AU, above the ν_6 resonance) to the five intermediate source regions used in the conventional NEA model in Bottke et al. (2002). For this paper 18,000 particles with $H < 18$ were created along with the revised NEA model by the courtesy of A. Morbidelli for the authors, and these particles were used for the numerical integrations described in the next sections.

Note that from the result of our previous study using the raw NEA population (Ito 2011), we are aware that the orbital distributions of the fainter NEAs, such as $H > 18$, are different from what the brighter NEA component yields. However, the diameter range of the crater record that

we are concerned is rather large, >5–10 km, which roughly corresponds to the brighter population of the current NEAs. Hence in this paper we do not consider the fainter components of NEAs than $H = 18$ in our numerical calculation. This criterion, however, can be of course changed depending on discovery and detection of more and more NEAs in various size ranges through large survey programs in the near future.

The orbital element distribution of the particles (18,000 each) belonging to the NEA populations A and B are shown in Fig. 1. In the panel (c) the excess of high inclination component is obvious, indicating the evident inclusion of the high inclination particles belonging to Hungaria and Phocaeas. Also, it is clear that the particles with larger semimajor axis (such as $a > 2.5$AU) are less frequent in the population B than in the population A, leading to a fact that there are more particles around $a \sim 1$AU in the population B. This difference is due to the difference in observational debiasing used in the new NEA model (Stuart 2001; Stuart & Binzel 2004), and will eventually have an influence on the difference in cratering asymmetry between the two populations (see Section 4. for detail).

For the numerical orbit integration scheme of these particles, we used the regularized mixed-variable symplectic method (Levison & Duncan 1994). The basic framework of our first stage simulation follows Ito & Malhotra (2006): When a test particle approaches within the physical radius of the Sun or that of planets, we consider the particle to have collided with that body and lost from the NEA population. Also, when the heliocentric distance of a test particle exceeds 100 AU, the particle is considered lost. Over the 100 Myr length of the simulation, a large fraction of the both populations would be expected to be removed in this way, and if this loss were not compensated, we would not be able to mimic a steady-state NEA flux. We realize the steady-state NEA flux in our numerical simulation as follows: for each "lost" particle, we immediately introduce in our simulation another particle with the original position and velocity of that "lost" particle. For example, when the particle i is removed from the simulation by any of the reasons described above at the position $\boldsymbol{r}_i$ with the velocity $\boldsymbol{v}_i$, another particle, also denoted by the subscript i, at the position $\boldsymbol{r}_{i,0}$ and with the velocity $\boldsymbol{v}_{i,0}$ is immediately introduced in the simulation where $\boldsymbol{r}_{i,0}$ and $\boldsymbol{v}_{i,0}$ are the initial position and the velocity of the particle i at the beginning of the integration.

3. Particle encounters with Earth's activity sphere

In our first stage numerical simulation described above, we recorded the encounters of particles at the Earth's activity sphere ($\sim$ 144 Earth radii) over the 100 Myr integration, and found a large number (several ten millions) of encounters with the Earth's activity sphere. In our simulation, average encounter velocities of the particles at the Earth's activity sphere are 22.36 km/s for the population A particles, and 22.25 km/s for the population B particles (see Fig. 2 for the encounter velocity distribution). We think the number of the encounters is large enough to establish an orbital distribution function of the particles that can be used to create "clones" of particles in order to increase the reliability of the collision statistics between the particles and the Earth or the Moon. Using the particle encounters at Earth's activity sphere, we generated cloned particles by perturbing the encounter position $\boldsymbol{r}$ and velocity $\boldsymbol{v}$ of each of the original particles so that their initial trajectories at the activity sphere become slightly different: $\boldsymbol{r}_{\rm clone} = (1+\delta_r)\boldsymbol{r}_{\rm original}$ and $\boldsymbol{v}_{\rm clone} = (1+\delta_v)\boldsymbol{v}_{\rm original}$, where δ_r and δ_v are random numbers in the range $[-0.1, 0.1]$. This procedure produces a large number of particles that obey nearly the same orbital distribution function as the original particles but with somewhat different paths toward the Earth and the Moon.

We repeated this cloning procedure five hundred times for all the results of the first stage numerical integrations, generating a large number of particle initial conditions on the Earth's activity sphere. Using these sets of cloned particles, we performed a second set of numerical integrations, this time with the restricted N-body problem including the Sun, the Earth, the Moon, and the cloned test particles. Here we did not include the effect of other planets than the Earth, but we included the Moon's gravity. All the cloned particles started near the Earth's activity sphere, and were integrated until they hit the Earth or the Moon or went out of the sphere. We used the present orbital elements of the Moon with true anomaly randomly chosen from 0 to 360° for each of the 500 sets of clones. We employed the regularized mixed-variable symplectic method again with a stepsize of 84.375 seconds ($= 2^{-10}$ days).

For the population A, the second stage calculations within the activity sphere of the Earth yielded 1,509,364 collisions with the Earth and 73,923 collisions with the Moon. For the population B, we have 1,155,955 collisions with the Earth and 64,604 collisions with the Moon. The ratio of the number of collisions with the Earth and those with the Moon is found to be 20.4 for the population A, and 17.9 for the population B. For comparison,

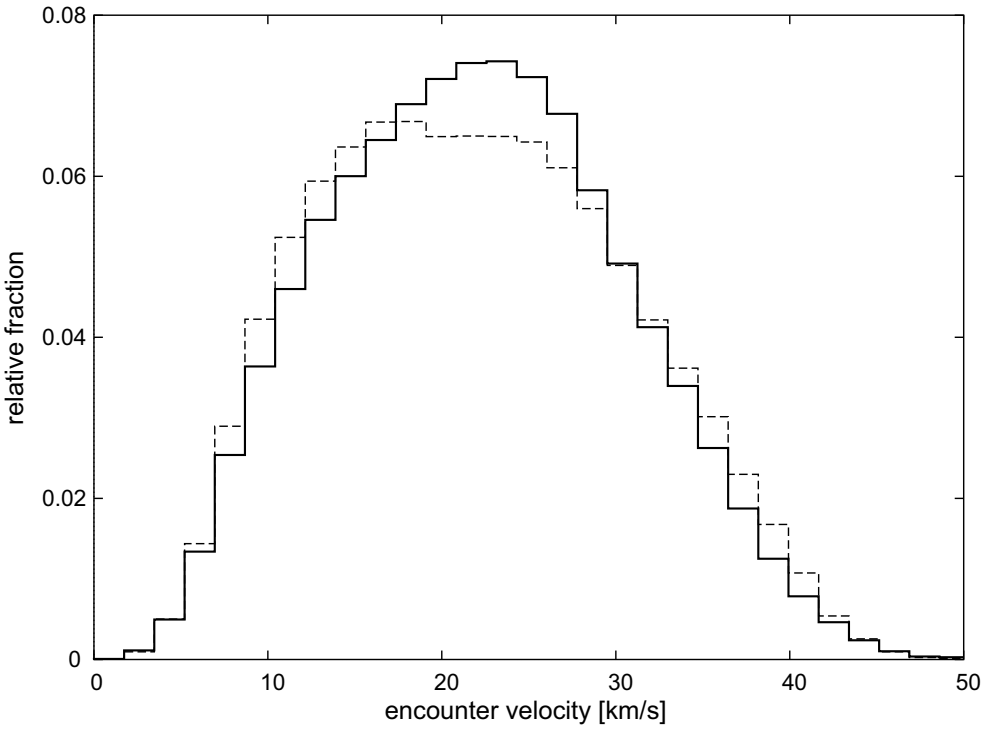

Figure 2. Fractional encounter velocity distribution at the Earth's activity sphere. The solid line is for the population A particles, and the dashed line is for the population B particles.

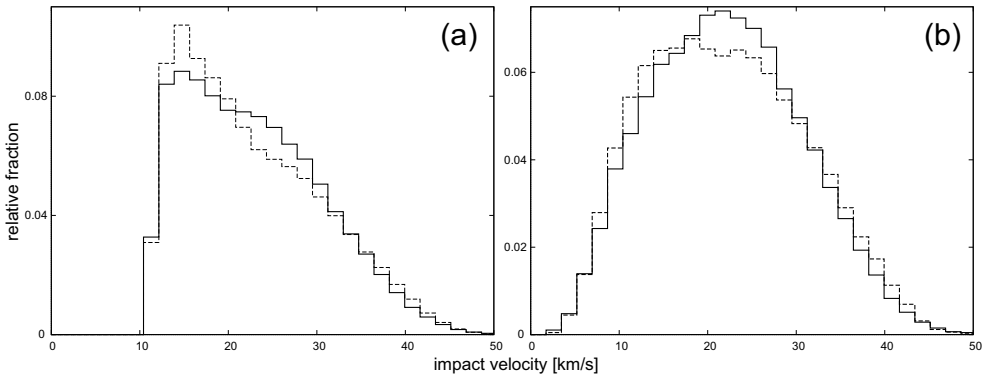

Figure 3. Distribution of impact velocity of the cloned particles on the Moon (a) and on the Earth (b). The solid lines are for the population A particles, and the dashed lines are for the population B particles.

we note that it has been reported that the ratio of collisional cross sections of the Earth and the Moon becomes ~ 23 by assuming isotropic collisions and average impact velocity of Earth-crossing asteroids to be 16.1 km/s on the Earth (Zahnle & Sleep 1997).

Fig. 3 shows the distribution of impact velocities of the clones on the Earth and on the Moon. Overall, the average impact velocities of the clones on the lunar surface (22.41 km/s for the population A, and 22.28 km/s for the population B) are almost the same as the average encounter velocity of the original particles at the Earth's activity sphere. This means that lunar gravity plays only a minor role in accelerating particles to the lunar surface in our numerical model.

4. Particle collisions with the Earth and the Moon

In order to compare the distribution of impacts in our numerical model with the actual lunar crater record, first we have to consider a correction to the raw numerical results due to the systematic difference in the impact velocities on the leading and trailing hemispheres, a difference that owes to the orbital motion of the satellite about its mother planet. For a satellite with synchronous rotation, the average impact velocity of projectiles is somewhat larger on the leading side than on the trailing side. This difference means that the apparent crater sizes would be larger on the leading side than on the trailing side (assuming the projectile size-frequency distribution (SFD) is not different on the two sides), resulting in the apparent increase (shift) in crater density on the leading side (Ishizaki & Furumoto

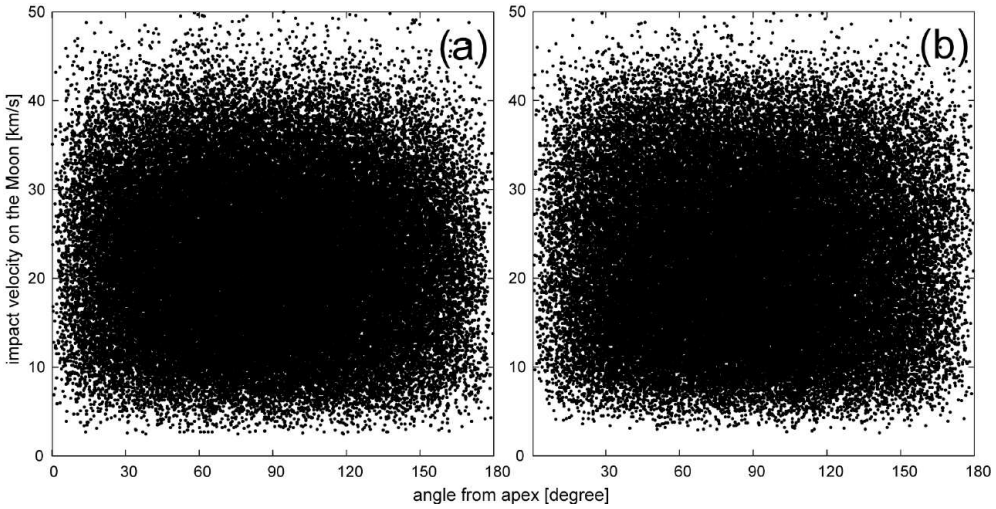

Figure 4. Dependence of the projectile impact velocity at the lunar surface ($v_{\rm imp}$, km/s) on the angular distance from apex (γ, degree). (a) For the population A, and (b) for the population B.

1997). The magnitude of the shift depends upon the relationship between the impact velocity $v_{\rm imp}$ and the crater size, D.

From the results of our second stage simulation, we computed the average impact velocity, $\langle v_{\rm imp}\rangle$ in km/s, of NEAs on the lunar surface as a function of angle from apex, γ (degrees), by a least squares fit (see Fig. 4 for the raw impact velocity data for the lunar collision). We find $\langle v_{\rm imp}\rangle = 22.9 - 0.00540\gamma$ for the population A, and $\langle v_{\rm imp}\rangle = 22.6 - 0.00333\gamma$ for the population B. This indicates that difference of $\langle v_{\rm imp}\rangle$ between the $\gamma = 90^\circ$ point and the apex ($\gamma = 0$) or antapex ($\gamma = 180^\circ$) is less than 0.486 km/s for the population A, less than 0.300 km/s for the population B. Compared with the average of $v_{\rm imp}$ over the entire range of $0 \leq \gamma \leq 180^\circ$, these velocity differences amount to $\lesssim 2.12\%$ for the population A, and $\lesssim 1.35\%$ for the population B, which are quite small in their effect on the crater number density change. This small difference is owed to the fact that the lunar orbital velocity of ~ 1 km/s is much lower than the average impact velocity $\langle v_{\rm imp}\rangle$. As a result of this small dependence, apparent change of the crater SFD due to the impact velocity difference between the leading side and the trailing side is quite modest.

Including this correction to our second stage simulation, we computed the simulated spatial density of NEA impacts on the Moon. Normalizing to unity at antapex, our simulation results for the crater density as functions of apex angle are shown in Fig. 5, panels (a) and (b). In Fig. 5, we used

a simple sinusoid with the function form of $\alpha + \beta \cos\gamma$ for a fitting curve where α and β are fitting parameters, normalizing $\alpha + \beta \cos 180^\circ = 1$.

For comparison, panel (c) shows the distribution found from the analysis of observed lunar rayed craters (Morota & Furumoto 2003). Note that the number of the lunar rayed craters in the observational data analyzed by Morota & Furumoto (2003) is only 222, while we have some 60,000 to 70,000 impacts in our simulations. This difference is reflected in the difference of the errorbar magnitudes in Fig. 5.

Examining Fig. 5, what we notice is that the apex/antapex asymmetry is less prominent in the numerical results (panels (a) and (b)) compared with the observed lunar rayed crater record (panel (c)). The maximum crater density at apex is about 1.65 (normalized to unity at antapex, and estimated from the best-fit sinusoid) in the observed crater record, whereas in our simulations, it is 1.31 ± 0.02 for the population A, and 1.34 ± 0.03 for the population B particles. This also means that the NEA population created by the new model (the population B) yields slightly stronger asymmetry in terms of the lunar impacts compared with what the NEA population created by the conventional model (the population A) does. But obviously the difference is not remarkable.

5. Summary and discussion

We carried out a new set of numerical integrations of a population of particles created by a new, revised debiased NEA flux model. The aim of our calculation is to search potentially "slower" objects which can reproduce the stronger cratering asymmetry on the Moon that has been actually observed for the lunar rayed craters; this is because the leading/trailing cratering asymmetry becomes more prominent when the average relative velocity between the Moon and the projectiles is low.

In our previous publications, we had performed similar numerical experiments using a debiased population of NEAs created by the conventional NEA flux model (Ito & Malhotra 2010). as well as a "raw" NEA population (Ito 2011). But either of the results did not reach the observed rayed cratering asymmetry. In this paper using a revised NEA flux model, the resulting relative crater density at apex became slightly larger than when we used the conventional NEA flux model. We suspect that this slight enhancement is caused by the fact that the particle population produced from the new NEA flux model (i.e. the population B) contains relatively more particles around the Earth, $a \sim 1$AU, than the population that was produced from the conventional NEA flux model (i.e. the population A)

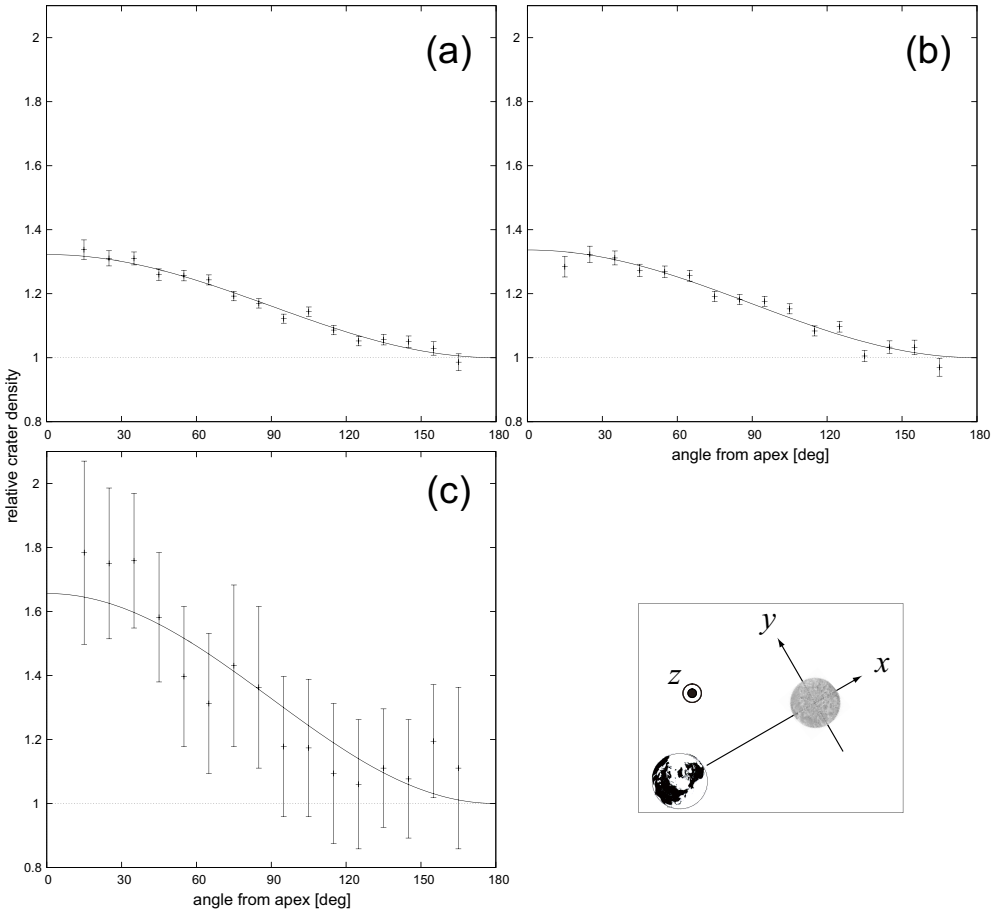

Figure 5. Modeled and observed impact crater distribution on the Moon. We normalized the crater density to unity at antapex ($\gamma = 180°$) using the best fit sinusoid (solid line curve). (a) Numerical result including the correction due to the difference of average impact velocity as a function of the angular distance (γ) from apex ($\gamma = 0$) for the population A particles. (b) Same as (a), but for the population B particles. (c) The observed rayed crater distribution of $D > 5$ km (Morota & Furumoto 3003). The inset at the bottom right illustrates the coordinate system in this frame: The Earth always lies along $-x$ direction, the Moon velocity is toward $+y$ direction, and $+z$ is the north of the Earth–Moon system. Apex point is defined as $(x, y, z) = (0, R_{\rm M}, 0)$ where $R_{\rm M}$ is the lunar radius.

does, as seen in Fig. 1. The closer-Earth NEA component has generally lower relative velocity with respect to the Earth/Moon system, hence creating a higher cratering asymmetry. The difference of the new and the conventional models is also characterized by the inclusion or no inclusion of the high inclination NEA component. But it does not have a significant effect on the final result of cratering asymmetry because the high inclination NEA component does not have a large collision probability on the Earth or the Moon due to their geometric configuration (i.e. inclined orbits).

Overall, difference between the results yielded by the new and conventional models is small, and we could not say that we have approached any explanation about the discrepancy between the crater record and what is suggested by the NEA dynamics. Hence, our result still implies the existence of undetected NEA populations with even lower relative velocity with respect to the Earth/Moon system. Deduced from the low relative velocity, this kind of populations could be Earth-coorbiting, some of them perhaps being produced by fragmentation due to Earth's tidal force when a projectile approaches the Earth–Moon system. Recently one of the very examples, the first Earth's Trojan object was detected through the survey observation by the WISE mission (Connors et al. 2011). In the forthcoming publications we will present our numerical result along the same computing scheme including slower NEA populations with several different dynamical characteristics including Earth's Lagrangian points, and will make an estimate as to what kind of NEA populations could be responsible for the lunar crater asymmetry as high as what is currently observed.

Of course, more complete observational surveys of NEAs will test our prediction, such as what is going on with Pan-STARRS. Also, future progress in the reconstruction of the true orbital distribution of NEAs by debiasing techniques, as well as reexamination of the lunar crater data including the latest lunar mission data, would be waited. Also, more careful examination as to how close to a steady-state the lunar impact flux has been is needed, as some large rayed craters are argued to be older than what they had been thought (Grier et al. 2001).

References

Bottke, W.F., Jedicke, R., Morbidelli, A., Vokrouhlický, D., Brož, M., Nesvorný, D., Petit, J.-M. & Gladman, B. 2000, *Science* **288**, 2190

Bottke, W.F., Morbidelli, A., Jedicke, R., Petit, J.-M., Levison, H.F., Michel, P. & Metcalfe, T.S. 2002, *Icarus* **156**, 399

Connors, M., Wiegert, P. & Veillet, C. 2011, *Nature* **475**, 481

Gallant, J., Gladman, B. & Ćuk, M. 2009, *Icarus* **202**, 371

Grier, J.A., McEwen, A.S., Lucey, P.G., Milazzo, M. & Strom, R.G. 2001, *J. Geophys. Res.* **106**, 32847

Horedt, G.P. & Neukum, G. 1984, *Icarus* **60**, 710

Ishizaki, Y. & Furumoto, M. 1997, *Planet. People* **6**, 12

Ito, T. & Malhotra, R. 2006, *Adv. Space Res.* **38**, 817

Ito, T. & Malhotra, R. 2010, *Astron. Astrophys.* **519**, A63

Ito, T., 2011, Asymmetric cratering on the moon: Case of the raw near-earth asteroid population, in *Advances in Geosciences,* **25**, ed. A. Bhardwaj (World Scientific, Singapore) pp. 109–119

Kawamura, T., Morota, T., Kobayashi, N. & Tanaka, S. 2011, *Geophys. Res. Lett.* **38**, p. L15201

Le Feuvre, M. & Wieczorek, M.A. 2008, *Icarus* **197**, 291

Le Feuvre, M. & Wieczorek, M.A. 2011, *Icarus* **214**, 1

Levison, H.F. & Duncan, M.J. 1994, *Icarus* **108**, 18

McEwen, A.S., Moore, J.M., & Shoemaker, E.M. 1997, *J. Geophys. Res.* **102**, 9231

Moon, H.-K., Byun, Y.-I., Yim, H.-S. & Raymond, S.N. 2008, *J. Korean Astron. Soc.* **41**, 7

Morota, T. & Furumoto, M. 2003, *Earth Planet. Sci. Lett.* **206**, 315

Schenk, P. & Sobieszczyk, S. 1999, *Bull. Am. Astron. Soc.* **31**, 1182

Shoemaker, E.M., Lucchitta, B.K., Wilhelms, D.E., Plescia, J.B., & Squyres, S.W. 1982, The geology of ganymede, in *Satellites of Jupiter*, ed. D. Morrison (The University of Arizona Press, Tucson) pp. 435–520

Stuart, J.S. 2001, *Science* **294**, 1691

Stuart J.S & Binzel, R.P. 2004, *Icarus* **170**, 295

Werner, S.C. & Medvedev, S. 2010, *Earth Planet. Sci. Lett.* **295**, 147

Zahnle, K,J. & Sleep, N.H. 1997, Impacts and the early evolution of life, in *Comets and the Origin and Evolution of Life*, eds. P.J. Thomas, C.F. Chyba and C.P. McKay (Springer–Verlag, New York) pp. 175–208

Zahnle, K.J., Dones, L. & Levison, H.F. 1998, *Icarus* **136**, 202

Zahnle, K.J., Schenk, P., Sobieszczyk, S., Dones, L., & Levison, H.F. 2001 *Icarus* **153**, 111